Observation of $e^+e^- \to \eta Y(2175)$ at center-of-mass energies above 3.7 GeV

M. Ablikim,[1] M. N. Achasov,[9,d] S. Ahmed,[14] X. C. Ai,[1] O. Albayrak,[5] M. Albrecht,[4] D. J. Ambrose,[45] A. Amoroso,[50a,50c] F. F. An,[1] Q. An,[47,38] J. Z. Bai,[1] O. Bakina,[23] R. Baldini Ferroli,[20a] Y. Ban,[31] D. W. Bennett,[19] J. V. Bennett,[5] N. Berger,[22] M. Bertani,[20a] D. Bettoni,[21a] J. M. Bian,[44] F. Bianchi,[50a,50c] E. Boger,[23,b] I. Boyko,[23] R. A. Briere,[5] H. Cai,[52] X. Cai,[1,38] O. Cakir,[41a] A. Calcaterra,[20a] G. F. Cao,[1,42] S. A. Cetin,[41b] J. Chai,[50c] J. F. Chang,[1,38] G. Chelkov,[23,b,c] G. Chen,[1] H. S. Chen,[1,42] J. C. Chen,[1] M. L. Chen,[1,38] S. Chen,[42] S. J. Chen,[29] X. Chen,[1,38] X. R. Chen,[26] Y. B. Chen,[1,38] X. K. Chu,[31] G. Cibinetto,[21a] H. L. Dai,[1,38] J. P. Dai,[34,h] A. Dbeyssi,[14] D. Dedovich,[23] Z. Y. Deng,[1] A. Denig,[22] I. Denysenko,[23] M. Destefanis,[50a,50c] F. De Mori,[50a,50c] Y. Ding,[27] C. Dong,[30] J. Dong,[1,38] L. Y. Dong,[1,42] M. Y. Dong,[1,38,42] Z. L. Dou,[29] S. X. Du,[54] P. F. Duan,[1] J. Z. Fan,[40] J. Fang,[1,38] S. S. Fang,[1,42] Y. Fang,[1] R. Farinelli,[21a,21b] L. Fava,[50b,50c] F. Feldbauer,[22] G. Felici,[20a] C. Q. Feng,[47,38] E. Fioravanti,[21a] M. Fritsch,[22,14] C. D. Fu,[1] Q. Gao,[1] X. L. Gao,[47,38] Y. Gao,[40] Z. Gao,[47,38] I. Garzia,[21a] K. Goetzen,[10] L. Gong,[30] W. X. Gong,[1,38] W. Gradl,[22] M. Greco,[50a,50c] M. H. Gu,[1,38] Y. T. Gu,[12] Y. H. Guan,[1] A. Q. Guo,[1] L. B. Guo,[28] R. P. Guo,[1] Y. Guo,[1] Y. P. Guo,[22] Z. Haddadi,[25] A. Hafner,[22] S. Han,[52] X. Q. Hao,[15] F. A. Harris,[43] K. L. He,[1,42] F. H. Heinsius,[4] T. Held,[4] Y. K. Heng,[1,38,42] T. Holtmann,[4] Z. L. Hou,[1] C. Hu,[28] H. M. Hu,[1,42] T. Hu,[1,38,42] Y. Hu,[1] G. S. Huang,[47,38] J. S. Huang,[15] X. T. Huang,[33] X. Z. Huang,[29] Z. L. Huang,[27] T. Hussain,[49] W. Ikegami Andersson,[51] Q. Ji,[1] Q. P. Ji,[15] X. B. Ji,[1,42] X. L. Ji,[1,38] L. W. Jiang,[52] X. S. Jiang,[1,38,42] X. Y. Jiang,[30] J. B. Jiao,[33] Z. Jiao,[17] D. P. Jin,[1,38,42] S. Jin,[1,42] T. Johansson,[51] A. Julin,[44] N. Kalantar-Nayestanaki,[25] X. L. Kang,[1] X. S. Kang,[30] M. Kavatsyuk,[25] B. C. Ke,[5] P. Kiese,[22] R. Kliemt,[10] B. Kloss,[22] O. B. Kolcu,[41b,f] B. Kopf,[4] M. Kornicer,[43] A. Kupsc,[51] W. Kühn,[24] J. S. Lange,[24] M. Lara,[19] P. Larin,[14] H. Leithoff,[22] C. Leng,[50c] C. Li,[51] Cheng Li,[47,38] D. M. Li,[54] F. Li,[1,38] F. Y. Li,[31] G. Li,[1] H. B. Li,[1,42] H. J. Li,[1] J. C. Li,[1] Jin Li,[32] Kang Li,[13] Ke Li,[1] Lei Li,[3] P. R. Li,[42,7] Q. Y. Li,[33] T. Li,[33] W. D. Li,[1,42] W. G. Li,[1] X. L. Li,[33] X. N. Li,[1,38] X. Q. Li,[30] Y. B. Li,[2] Z. B. Li,[39] H. Liang,[47,38] Y. F. Liang,[36] Y. T. Liang,[24] G. R. Liao,[11] D. X. Lin,[14] B. Liu,[34,h] B. J. Liu,[1] C. X. Liu,[1] D. Liu,[47,38] F. H. Liu,[35] Fang Liu,[1] Feng Liu,[6] H. B. Liu,[12] H. M. Liu,[1,42] Huanhuan Liu,[1] Huihui Liu,[16] J. Liu,[1] J. B. Liu,[47,38] J. P. Liu,[52] J. Y. Liu,[1] K. Liu,[40] K. Y. Liu,[27] L. D. Liu,[31] P. L. Liu,[1,38] Q. Liu,[42] S. B. Liu,[47,38] X. Liu,[26] Y. B. Liu,[30] Y. Y. Liu,[30] Z. A. Liu,[1,38,42] Zhiqing Liu,[22] H. Loehner,[25] Y. F. Long,[31] X. C. Lou,[1,38,42] H. J. Lu,[17] J. G. Lu,[1,38] Y. Lu,[1] Y. P. Lu,[1,38] C. L. Luo,[28] M. X. Luo,[53] T. Luo,[43] X. L. Luo,[1,38] X. R. Lyu,[42] F. C. Ma,[27] H. L. Ma,[1] L. L. Ma,[33] M. M. Ma,[1] Q. M. Ma,[1] T. Ma,[1] X. N. Ma,[30] X. Y. Ma,[1,38] Y. M. Ma,[33] F. E. Maas,[14] M. Maggiora,[50a,50c] Q. A. Malik,[49] Y. J. Mao,[31] Z. P. Mao,[1] S. Marcello,[50a,50c] J. G. Messchendorp,[25] G. Mezzadri,[21b] J. Min,[1,38] T. J. Min,[1] R. E. Mitchell,[19] X. H. Mo,[1,38,42] Y. J. Mo,[6] C. Morales Morales,[14] G. Morello,[20a] N. Yu. Muchnoi,[9,d] H. Muramatsu,[44] P. Musiol,[4] Y. Nefedov,[23] F. Nerling,[10] I. B. Nikolaev,[9,d] Z. Ning,[1,38] S. Nisar,[8] S. L. Niu,[1,38] X. Y. Niu,[1] S. L. Olsen,[32] Q. Ouyang,[1,38,42] S. Pacetti,[20b] Y. Pan,[47,38] M. Papenbrock,[51] P. Patteri,[20a] M. Pelizaeus,[4] H. P. Peng,[47,38] K. Peters,[10,g] J. Pettersson,[51] J. L. Ping,[28] R. G. Ping,[1,42] R. Poling,[44] V. Prasad,[1] H. R. Qi,[2] M. Qi,[29] S. Qian,[1,38] C. F. Qiao,[42] L. Q. Qin,[33] N. Qin,[52] X. S. Qin,[1] Z. H. Qin,[1,38] J. F. Qiu,[1] K. H. Rashid,[49,i] C. F. Redmer,[22] M. Ripka,[22] G. Rong,[1,42] Ch. Rosner,[14] X. D. Ruan,[12] A. Sarantsev,[23,e] M. Savrié,[21b] C. Schnier,[4] K. Schoenning,[51] W. Shan,[31] M. Shao,[47,38] C. P. Shen,[2] P. X. Shen,[30] X. Y. Shen,[1,42] H. Y. Sheng,[1] W. M. Song,[1] X. Y. Song,[1] S. Sosio,[50a,50c] S. Spataro,[50a,50c] G. X. Sun,[1] J. F. Sun,[15] S. S. Sun,[1,42] X. H. Sun,[1] Y. J. Sun,[47,38] Y. Z. Sun,[1] Z. J. Sun,[1,38] Z. T. Sun,[19] C. J. Tang,[36] X. Tang,[1] I. Tapan,[41c] E. H. Thorndike,[45] M. Tiemens,[25] I. Uman,[41d] G. S. Varner,[43] B. Wang,[30] B. L. Wang,[42] D. Wang,[31] D. Y. Wang,[31] K. Wang,[1,38] L. L. Wang,[1] L. S. Wang,[1] M. Wang,[33] P. Wang,[1] P. L. Wang,[1] W. Wang,[1,38] W. P. Wang,[47,38] X. F. Wang,[40] Y. Wang,[37] Y. D. Wang,[14] Y. F. Wang,[1,38,42] Y. Q. Wang,[22] Z. Wang,[1,38] Z. G. Wang,[1,38] Z. Y. Wang,[1] Zongyuan Wang,[1] T. Weber,[22] D. H. Wei,[11] P. Weidenkaff,[22] S. P. Wen,[1] U. Wiedner,[4] M. Wolke,[51] L. H. Wu,[1] L. J. Wu,[1] Z. Wu,[1,38] L. Xia,[47,38] L. G. Xia,[40] Y. Xia,[18] D. Xiao,[1] H. Xiao,[48] Z. J. Xiao,[28] Y. G. Xie,[1,38] Y. H. Xie,[6] Q. L. Xiu,[1,38] G. F. Xu,[1] J. J. Xu,[1] L. Xu,[1] Q. J. Xu,[13] Q. N. Xu,[42] X. P. Xu,[37] L. Yan,[50a,50c] W. B. Yan,[47,38] Y. H. Yan,[18] H. J. Yang,[34,h] H. X. Yang,[1] L. Yang,[52] Y. X. Yang,[11] M. Ye,[1,38] M. H. Ye,[7] J. H. Yin,[1] Z. Y. You,[39] B. X. Yu,[1,38,42] C. X. Yu,[30] J. S. Yu,[26] C. Z. Yuan,[1,42] Y. Yuan,[1] A. Yuncu,[41b,a] A. A. Zafar,[49] Y. Zeng,[18] Z. Zeng,[47,38] B. X. Zhang,[1] B. Y. Zhang,[1,38] C. C. Zhang,[1] D. H. Zhang,[1] H. H. Zhang,[39] H. Y. Zhang,[1,38] J. Zhang,[1] J. J. Zhang,[1] J. L. Zhang,[1] J. Q. Zhang,[1] J. W. Zhang,[1,38,42] J. Y. Zhang,[1] J. Z. Zhang,[1,42] K. Zhang,[1] L. Zhang,[1] S. Q. Zhang,[30] X. Y. Zhang,[33] Y. H. Zhang,[1,38] Y. N. Zhang,[42] Y. T. Zhang,[47,38] Yang Zhang,[1] Yao Zhang,[1] Yu Zhang,[42] Z. H. Zhang,[6] Z. P. Zhang,[47] Z. Y. Zhang,[52] G. Zhao,[1] J. W. Zhao,[1,38] J. Y. Zhao,[1] J. Z. Zhao,[1,38] Lei Zhao,[47,38] Ling Zhao,[1] M. G. Zhao,[30] Q. Zhao,[1] Q. W. Zhao,[1] S. J. Zhao,[54] T. C. Zhao,[1] Y. B. Zhao,[1,38] Z. G. Zhao,[47,38] A. Zhemchugov,[23,b] B. Zheng,[48,14] J. P. Zheng,[1,38] W. J. Zheng,[33] Y. H. Zheng,[42] B. Zhong,[28] L. Zhou,[1,38] X. Zhou,[52] X. K. Zhou,[47,38] X. R. Zhou,[47,38] X. Y. Zhou,[1] K. Zhu,[1] K. J. Zhu,[1,38,42] S. Zhu,[1] S. H. Zhu,[46] X. L. Zhu,[40] Y. C. Zhu,[47,38] Y. S. Zhu,[1,42] Z. A. Zhu,[1,42] J. Zhuang,[1,38] L. Zotti,[50a,50c] B. S. Zou,[1] and J. H. Zou[1]

(BESIII Collaboration)

[1]*Institute of High Energy Physics, Beijing 100049, People's Republic of China*
[2]*Beihang University, Beijing 100191, People's Republic of China*
[3]*Beijing Institute of Petrochemical Technology, Beijing 102617, People's Republic of China*
[4]*Bochum Ruhr-University, D-44780 Bochum, Germany*
[5]*Carnegie Mellon University, Pittsburgh, Pennsylvania 15213, USA*
[6]*Central China Normal University, Wuhan 430079, People's Republic of China*
[7]*China Center of Advanced Science and Technology, Beijing 100190, People's Republic of China*
[8]*COMSATS Institute of Information Technology, Lahore, Defence Road, Off Raiwind Road, 54000 Lahore, Pakistan*
[9]*G.I. Budker Institute of Nuclear Physics SB RAS (BINP), Novosibirsk 630090, Russia*
[10]*GSI Helmholtzcentre for Heavy Ion Research GmbH, D-64291 Darmstadt, Germany*
[11]*Guangxi Normal University, Guilin 541004, People's Republic of China*
[12]*Guangxi University, Nanning 530004, People's Republic of China*
[13]*Hangzhou Normal University, Hangzhou 310036, People's Republic of China*
[14]*Helmholtz Institute Mainz, Johann-Joachim-Becher-Weg 45, D-55099 Mainz, Germany*
[15]*Henan Normal University, Xinxiang 453007, People's Republic of China*
[16]*Henan University of Science and Technology, Luoyang 471003, People's Republic of China*
[17]*Huangshan College, Huangshan 245000, People's Republic of China*
[18]*Hunan University, Changsha 410082, People's Republic of China*
[19]*Indiana University, Bloomington, Indiana 47405, USA*
[20a]*INFN Laboratori Nazionali di Frascati, I-00044 Frascati, Italy*
[20b]*INFN and University of Perugia, I-06100 Perugia, Italy*
[21a]*INFN Sezione di Ferrara, I-44122 Ferrara, Italy*
[21b]*University of Ferrara, I-44122 Ferrara, Italy*
[22]*Johannes Gutenberg University of Mainz, Johann-Joachim-Becher-Weg 45, D-55099 Mainz, Germany*
[23]*Joint Institute for Nuclear Research, 141980 Dubna, Moscow Region, Russia*
[24]*Justus-Liebig-Universitaet Giessen, II. Physikalisches Institut, Heinrich-Buff-Ring 16, D-35392 Giessen, Germany*
[25]*KVI-CART, University of Groningen, NL-9747 AA Groningen, The Netherlands*
[26]*Lanzhou University, Lanzhou 730000, People's Republic of China*
[27]*Liaoning University, Shenyang 110036, People's Republic of China*
[28]*Nanjing Normal University, Nanjing 210023, People's Republic of China*
[29]*Nanjing University, Nanjing 210093, People's Republic of China*
[30]*Nankai University, Tianjin 300071, People's Republic of China*
[31]*Peking University, Beijing 100871, People's Republic of China*
[32]*Seoul National University, Seoul, 151-747 Korea*
[33]*Shandong University, Jinan 250100, People's Republic of China*
[34]*Shanghai Jiao Tong University, Shanghai 200240, People's Republic of China*
[35]*Shanxi University, Taiyuan 030006, People's Republic of China*
[36]*Sichuan University, Chengdu 610064, People's Republic of China*
[37]*Soochow University, Suzhou 215006, People's Republic of China*
[38]*State Key Laboratory of Particle Detection and Electronics, Beijing 100049, Hefei 230026, People's Republic of China*
[39]*Sun Yat-Sen University, Guangzhou 510275, People's Republic of China*
[40]*Tsinghua University, Beijing 100084, People's Republic of China*
[41a]*Ankara University, 06100 Tandogan, Ankara, Turkey*
[41b]*Istanbul Bilgi University, 34060 Eyup, Istanbul, Turkey*
[41c]*Uludag University, 16059 Bursa, Turkey*
[41d]*Near East University, Nicosia, North Cyprus, Mersin 10, Turkey*
[42]*University of Chinese Academy of Sciences, Beijing 100049, People's Republic of China*
[43]*University of Hawaii, Honolulu, Hawaii 96822, USA*
[44]*University of Minnesota, Minneapolis, Minnesota 55455, USA*
[45]*University of Rochester, Rochester, New York 14627, USA*
[46]*University of Science and Technology Liaoning, Anshan 114051, People's Republic of China*
[47]*University of Science and Technology of China, Hefei 230026, People's Republic of China*
[48]*University of South China, Hengyang 421001, People's Republic of China*
[49]*University of the Punjab, Lahore-54590, Pakistan*

[50a]University of Turin, I-10125 Turin, Italy
[50b]University of Eastern Piedmont, I-15121 Alessandria, Italy
[50c]INFN, I-10125 Turin, Italy
[51]Uppsala University, Box 516, SE-75120 Uppsala, Sweden
[52]Wuhan University, Wuhan 430072, People's Republic of China
[53]Zhejiang University, Hangzhou 310027, People's Republic of China
[54]Zhengzhou University, Zhengzhou 450001, People's Republic of China

(Received 14 September 2017; published 31 January 2019)

The state $Y(2175)$ is observed in the process $e^+e^- \to \eta Y(2175)$ with a statistical significance larger than 10 standard deviations using the data collected with the BESIII detector operating at the BEPCII storage ring at center-of-mass energies between 3.7 and 4.6 GeV. This is the first observation of the $Y(2175)$ in this process. The mass and width of the $Y(2175)$ are determined to be $(2135 \pm 8 \pm 9)$ MeV/c^2 and $(104 \pm 24 \pm 12)$ MeV, respectively, and the production cross section (σ) of $e^+e^- \to \eta Y(2175) \to \eta\phi f_0(980) \to \eta\phi\pi^+\pi^-$ is at the several hundred femtobarn level. No significant signal for the process $e^+e^- \to \eta' Y(2175)$ is observed and the upper limit on $\sigma(e^+e^- \to \eta' Y(2175))/\sigma(e^+e^- \to \eta Y(2175))$ is estimated to be 0.43 at the 90% confidence level. We also search for $\psi(3686) \to \eta Y(2175)$. No significant signal is observed, indicating a strong suppression relative to the corresponding J/ψ decay, in violation of the "12% rule".

DOI: 10.1103/PhysRevD.99.012014

I. INTRODUCTION

The $Y(2175)$, which is notated as $\phi(2170)$ in Ref. [1], was first observed in 2006 by the *BABAR* Collaboration [2] via the initial-state-radiation (ISR) process $e^+e^- \to \gamma_{\rm ISR}\phi f_0(980)$ with a mass of $(2175 \pm 10 \pm 15)$ MeV/c^2 and a decay width of $(58 \pm 16 \pm 20)$ MeV. It was subsequently confirmed by the Belle Collaboration in the same process [3] and by the BESII and BESIII collaborations in J/ψ hadronic decays [4,5]. The *BABAR* Collaboration updated their analysis in 2012 with improved statistics [6].

Behaving similarly to the $Y(4260)$ in the charm sector and the $\Upsilon(10860)$ in the bottom sector, the $Y(2175)$ is regarded as a candidate for a tetraquark state [7,8], a strangeonium hybrid state [9], or a conventional $s\bar{s}$ state [10,11]. The quark model [12–14] predicts two conventional $s\bar{s}$ states near 2175 MeV/c^2, 3^3S_1 and 2^3D_1, but both of them are significantly broader than the $Y(2175)$, which makes the $Y(2175)$ more mysterious.

Despite all previous experimental and theoretical effort, our knowledge of the $Y(2175)$ is still very limited. Its observed production mechanisms are so far limited to direct e^+e^- annihilation and $J/\psi \to \eta Y(2175)$ decay. Furthermore, there are inconsistencies in previous mass and width measurements [3,5,6].

Since the process $J/\psi \to \eta Y(2175)$ has been observed [4,5], it is natural to expect the production of $\eta Y(2175)$ in $\psi(3686)$ decays as well as in direct e^+e^- annihilation in the nonresonant energy regions. The η is a mixture of the pseudoscalar SU(3) octet and singlet states; therefore the other mixture partner, η', is also expected to accompany the production of the $Y(2175)$ when the center-of-mass (c.m.) energy ($\sqrt{s}$) of e^+e^- annihilation is above the production threshold. BESIII has accumulated the world's largest data samples at the $\psi(3686)$ peak and at higher energies up to 4.6 GeV, which gives us a good opportunity to search for these processes.

Recently, several charged quarkoniumlike states Z_c [15–18] and Z_b [19] have been observed through decays of the $Y(4260)$, $\Upsilon(10860)$ or other charmoniumlike or bottomoniumlike states. One may expect similar charged strangeoniumlike states produced in $Y(2175) \to \phi\pi^+\pi^-$ decays, considering the similarity of the $Y(2175)$, $Y(4260)$,

[a]Also at Bogazici University, 34342 Istanbul, Turkey.
[b]Also at the Moscow Institute of Physics and Technology, Moscow 141700, Russia.
[c]Also at the Functional Electronics Laboratory, Tomsk State University, Tomsk 634050, Russia.
[d]Also at the Novosibirsk State University, Novosibirsk 630090, Russia.
[e]Also at the NRC "Kurchatov Institute," PNPI, 188300 Gatchina, Russia.
[f]Also at Istanbul Arel University, 34295 Istanbul, Turkey.
[g]Also at Goethe University Frankfurt, 60323 Frankfurt am Main, Germany.
[h]Also at Key Laboratory for Particle Physics, Astrophysics and Cosmology, Ministry of Education; Shanghai Key Laboratory for Particle Physics and Cosmology; Institute of Nuclear and Particle Physics, Shanghai 200240, People's Republic of China.
[i]Also at Government College Women University, Sialkot—51310 Punjab, Pakistan.

TABLE I. Summary of the data samples and the cross section measurements of $e^+e^- \to \eta Y(2175) \to \eta\phi f_0(980) \to \eta\phi\pi^+\pi^-$. Here $\sqrt{s}$ is the c.m. energy, $\mathcal{L}_{\rm int}$ is the integrated luminosity, $N^{\rm obs}$ is the number of observed signal events from the simultaneous fit described in the text, $(1+\delta)\cdot\epsilon$ (as described in Sec. IV) is the product of the ISR correction factor and signal reconstruction efficiency. The correction factors of vacuum polarization, $1+\delta^{\rm vac}$ (as described in Sec. IV), are listed except for $\sqrt{s} = 3.686$ GeV since the contribution of vacuum polarization is included in the parameters of the $\psi(3686)$. Born cross sections $\sigma^{\rm B}$ are listed with statistical (first) and systematic (second) uncertainties. The last column is the corresponding statistical significance for each data sample.

$\sqrt{s}$ (GeV)	$\mathcal{L}_{\rm int}$ (pb^{-1})	$N^{\rm obs}$	$(1+\delta)\cdot\epsilon$	$1+\delta^{vac}$	$\sigma^{\rm B}$ (pb)	Significance
3.686	666	19.0 ± 9.0	0.0861	⋯	$1.72 \pm 0.82 \pm 1.00$	1.5σ
3.773	2917	47.4 ± 9.1	0.0865	1.057	$0.93 \pm 0.18 \pm 0.15$	6.2σ
4.008	482	3.8 ± 2.6	0.0976	1.044	$0.40 \pm 0.27 \pm 0.34$	1.0σ
4.226	1092	12.3 ± 4.1	0.1052	1.056	$0.53 \pm 0.17 \pm 0.05$	3.8σ
4.258	826	11.6 ± 3.7	0.1067	1.054	$0.65 \pm 0.21 \pm 0.08$	4.2σ
4.358	540	6.4 ± 2.7	0.1113	1.051	$0.53 \pm 0.22 \pm 0.07$	2.9σ
4.416	1029	10.8 ± 4.1	0.1135	1.053	$0.46 \pm 0.17 \pm 0.21$	3.2σ
4.600	567	2.7 ± 1.9	0.1164	1.055	$0.20 \pm 0.14 \pm 0.02$	1.5σ

and $\Upsilon(10860)$. The authors of Ref. [20] predict the existence of a sharp peaking structure (Z_{s1}) close to the $K\bar{K}^*$ threshold and a broad structure (Z_{s2}) close to the $K^*\bar{K}^*$ threshold in the $\phi\pi$ mass spectrum. These can be searched for using the decays of the $Y(2175)$ produced in $e^+e^- \to \eta Y(2175)$ and $\eta' Y(2175)$.

In this article, we present the first observation of $e^+e^- \to \eta Y(2175)$ and measurement of its production cross sections, a search for $e^+e^- \to \eta' Y(2175)$ and an estimation of the upper limit of the production rate at the c.m. energies [21] from 3.686 to 4.6 GeV, and a search for $\psi(3686) \to \eta Y(2175)$ and determination of the upper limit on the branching fraction, as listed in Table I with the corresponding integrated luminosities $\mathcal{L}$ [22].

The remainder of this paper is organized as follows. In Sec. II, the BESIII detector and the data samples are described. In Sec. III, the event selections for $e^+e^- \to \eta Y(2175)$ are listed. Section IV presents the determination of the signal yield and the cross section measurement, as well as the measurement of the resonance parameters of the $Y(2175)$ in $e^+e^- \to \eta Y(2175)$, while Secs. V and VI show the search for the Z_s and $\psi(3686) \to \eta Y(2175)$, respectively. Section VII shows the search for $e^+e^- \to \eta' Y(2175)$. Section VIII lists the estimation of the systematic uncertainties. A summary of all results is given in Sec. IX.

II. BESIII DETECTOR AND DATA SAMPLES

The BESIII detector, described in detail in Ref. [23], has a geometrical acceptance of 93% of 4πsr. A small-cell helium-based main drift chamber (MDC) provides a charged particle momentum resolution of 0.5% at 1 GeV/c in a 1 T magnetic field and supplies specific ionization energy loss (dE/dx) measurements with a resolution better than 6% for electrons from Bhabha scattering. The electromagnetic calorimeter (EMC) measures photon energies with a resolution of 2.5% (5%) at 1.0 GeV in the barrel (end caps). Particle identification (PID) is provided by a time-of-flight system (TOF) with a time resolution of 80 ps (110 ps) for the barrel (end caps). The muon system, located in the iron flux return yoke of the magnet, provides 2 cm position resolution and detects muon tracks with momentum greater than 0.5 GeV/c.

The data used in this analysis are listed in Table I, where the data sample at $\sqrt{s} = 3.686$ GeV corresponds to the $\psi(3686)$ data sample of $(448.1 \pm 2.9) \times 10^6$ events in total and contains two subsamples of $(107.0 \pm 0.8) \times 10^6$ and $(341.1 \pm 2.1) \times 10^6$ [24] events collected in 2009 and 2012, respectively. The data at the other energies were taken during 2009 and 2015.

The GEANT4-based [25] Monte Carlo (MC) simulation software BOOST [26] includes the geometric description of the BESIII detector and a simulation of the detector response. It is used to optimize the event selection criteria, estimate backgrounds and evaluate the reconstruction efficiency. For each energy point, signal MC samples of $e^+e^- \to \eta Y(2175)$ with $Y(2175) \to \phi f_0(980) \to \phi\pi^+\pi^-$, $\phi \to K^+K^-$ and $\eta \to \gamma\gamma$ are generated, and $\eta Y(2175)$ is generated with an angular distribution of $1 + \cos^2\theta$ where θ is the polar angle in the e^+e^- c.m. frame. For the decays of intermediate states, both the $Y(2175) \to \phi f_0(980)$ and $\eta \to \gamma\gamma$ are generated evenly in phase space, and the $\phi \to K^+K^-$ is generated using the VSS model in EVTGEN [27,28], which describes the two-body decays of a vector particle to two pseudoscalar ones. The resonance parameters of the $Y(2175)$ are taken from the measurement in this analysis, and the $f_0(980)$ is parametrized with the Flatté formula [29], with parameters determined from the BESII measurement [30]. The ISR is simulated with KKMC [31], and the final state radiation (FSR) is handled with PHOTOS [32]. The process $e^+e^- \to \eta' Y(2175)$ is simulated at each energy point with a similar procedure, and the decay $\eta' \to \gamma\pi^+\pi^-$ is generated as $\eta' \to \gamma\rho^0$ with $\rho^0 \to \pi^+\pi^-$ [33].

For background studies, two inclusive MC samples of e^+e^- annihilation processes with the integrated luminosities equivalent to those of data are generated at $\sqrt{s} =$ 3.686 and 3.773 GeV. The physics processes should be similar at the other energy points. In these samples the $\psi(3686)$ and $\psi(3770)$ are allowed to decay generically, with the main known decay channels being generated using EVTGEN [27] with branching fractions set to the world average values [1]. The remaining events associated with charmonium decays are generated with LUNDCHARM [34] while continuum hadronic events are generated with PYTHIA [35]. For the QED events, $e^+e^- \to \tau^+\tau^-$ is generated with KKMC [31], the two-photon process is generated with TWOGAM [36] and other events are generated with BABAYAGA [37].

III. EVENT SELECTIONS

For the study of $e^+e^- \to \eta Y(2175)$, we expect four charged particles with zero net charge and two photons in the final state.

Each charged track is required to have its point of closest approach to the beamline within 1 cm in the radial direction and within 10 cm from the interaction point along the beam direction, and to lie within the polar angle coverage of the MDC, $|\cos\theta| < 0.93$ in the laboratory frame. PID for charged tracks is based on combining the dE/dx and TOF information. The PID confidence levels, $\mathrm{Pro}_{\mathrm{bPID}}(i)$, are calculated for each charged track for each particle hypothesis i of pion and kaon. If $\mathrm{Pro}_{\mathrm{bPID}}(K)$ is larger than $\mathrm{Pro}_{\mathrm{bPID}}(\pi)$ and $\mathrm{Pro}_{\mathrm{bPID}}(K)$ is larger than 0.001, the track is regarded as a kaon; otherwise it is taken as a pion. Two identified kaon and pion candidate pairs with opposite charges are required.

Photons are reconstructed from showers in the EMC which are isolated from charged tracks by at least 10 degrees. A good photon candidate is required to have an energy of at least 25 MeV in the barrel ($|\cos\theta| < 0.80$) or 50 MeV in the end caps ($0.86 < |\cos\theta| < 0.92$). In order to suppress electronic noise and energy deposits unrelated to the event, the EMC time t of the photon candidate must be in coincidence with the event start time in the range $0 \le t \le 700$ ns. The η candidate is reconstructed using the two most energetic photons.

A four-constraint (4C) kinematic fit, which constrains the sum of the four-momentum of all particles in the final state to be that of the initial e^+e^- system, is performed for the $\gamma\gamma\pi^+\pi^-K^+K^-$ system to get a better resolution and background suppression. The χ^2 of the kinematic fit is shown in Fig. 1(a) and is required to be less than 60.

After all the above selection criteria are applied, we use mass windows around the η and ϕ, numerically $[0.513, 0.578]$ GeV/c^2 in the $\gamma\gamma$ invariant mass and $[1.009, 1.031]$ GeV/c^2 in the K^+K^- invariant mass, respectively, to select signal events. The $\pi^+\pi^-$ system in $Y(2175) \to \phi\pi^+\pi^-$ decays tends to have $J^{PC} = 0^{++}$ and is dominated by $f_0(980)$. Figure 2 shows the scatter plot of $\pi^+\pi^-$ versus $\phi\pi^+\pi^-$ invariant masses for the sum of the data samples with $\sqrt{s} > 3.7$ GeV. A clear cluster corresponding to the $Y(2175) \to \phi f_0(980)$ events is clearly visible. Only events in the mass window of the $f_0(980)$ ($[0.868, 1.089]$ GeV/c^2 in the $\pi^+\pi^-$ invariant mass) are used for the cross section measurement. The mass windows used above are defined as $[\mu - 1.5 \cdot W, \mu + 1.5 \cdot W]$, where μ and W are the mean value and full width at half maximum (FWHM), respectively, of the invariant mass distributions of the signal MC simulation. Analogously, the corresponding sideband regions are defined as $[\mu - 5 \cdot W, \mu - 2 \cdot W]$ and $[\mu + 2 \cdot W, \mu + 5 \cdot W]$, which are twice as wide as the signal region. Figure 1 shows the invariant mass distributions of $\gamma\gamma$ (b), $\pi^+\pi^-$ (c) and K^+K^- (d) for the data sample and the inclusive and signal MC simulation samples taken or generated at $\sqrt{s} = 3.773$ GeV. Here all the event selections are applied except the one on the plotted variable.

The invariant mass distributions of $\phi f_0(980)$ for the seven data samples with $\sqrt{s} > 3.7$ GeV are shown individually in Fig. 3. We leave the analysis of the data sample at $\sqrt{s} = 3.686$ GeV to Sec. VI and focus on energy points with $\sqrt{s} > 3.7$ GeV here. The $Y(2175)$ signal can be observed over a smooth background level, especially for the data sample at $\sqrt{s} = 3.773$ GeV, where the integrated luminosity is the largest. The invariant mass distribution of

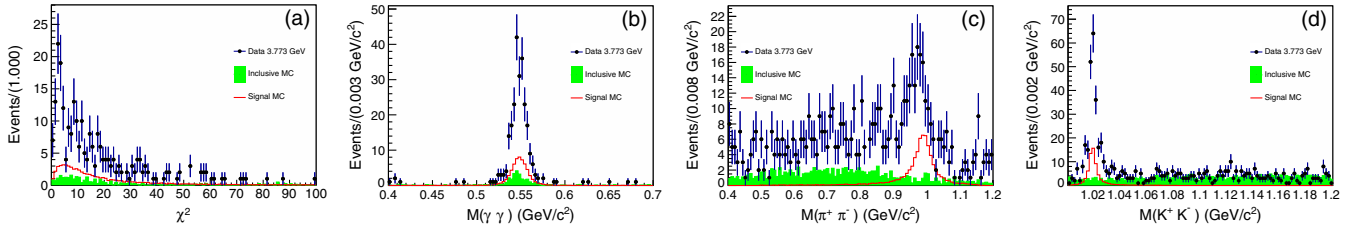

FIG. 1. The distributions of χ^2 from 4C kinematic fit (a), invariant masses of $\gamma\gamma$ (b), $\pi^+\pi^-$ (c) and K^+K^- (d) for the data samples (points), the inclusive (green hatch) and the signal (red line) MC simulation samples taken or generated at $\sqrt{s} = 3.773$ GeV. The discrepancies between data and MC simulation come from the non-$Y(2175)$ processes described in the text.

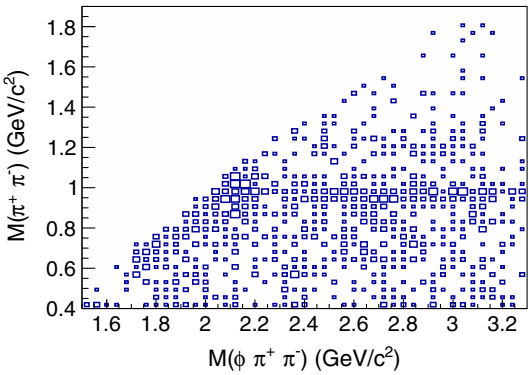

FIG. 2. Scatter plot of $\pi^+\pi^-$ versus $\phi\pi^+\pi^-$ invariant masses for the sum of data samples with $\sqrt{s} > 3.7$ GeV.

$\phi f_0(980)$ summing over the seven data samples with $\sqrt{s} > 3.7$ GeV is also shown in Fig. 3.

The inclusive MC sample at $\sqrt{s} = 3.773$ GeV is used to check for possible backgrounds. No peaking background is found and the main background is the non-$Y(2175)$ process $e^+e^- \to \eta K^+K^-\pi^+\pi^-$, including both the $\eta\phi\pi^+\pi^-$ and $\eta K^+K^- f_0(980)$ processes. There are almost no other backgrounds around the $Y(2175)$ peak area. Exclusive MC samples of the non-$Y(2175)$ processes are generated with 100,000 events at each c.m. energy, and the shapes are used to describe the background in the fit to the invariant mass distributions. Events in the sideband regions of the $f_0(980)$ and ϕ from data are used to check for the presence of peaking background, and the corresponding distributions are shown in Fig. 3.

IV. SIGNAL YIELDS AND BORN CROSS SECTIONS

We use an unbinned maximum likelihood method to fit the $\phi f_0(980)$ invariant mass spectra in order to extract the yields of signal events and the $Y(2175)$ resonance parameters. A simultaneous fit is applied to all the data samples with $\sqrt{s} > 3.7$ GeV. The same functional form, a modified Breit-Wigner function convolved with a resolution function, is used to describe the signal at different energy points, which is

$$\left(\left|\frac{M\Gamma}{M^2 - m^2 - iM\Gamma}\right|^2 \cdot \frac{\Phi(m)}{\Phi(M)} \cdot \epsilon(m)\right) \otimes G(m; 0, \sigma), \quad (1)$$

where M and Γ are the mass and decay width of the $Y(2175)$, respectively; G is a Gaussian function with a mean fixed to zero and a standard deviation σ to describe the mass resolution; m is the invariant mass of $\phi f_0(980)$; $\epsilon(m)$ is the mass-dependent efficiency determined from MC simulation. The term $\Phi(m) = (\frac{|p|}{\sqrt{s}})^3$ is the two-body phase space factor for a P-wave system, where p is the momentum of $Y(2175)$ in the e^+e^- rest frame. The background shape is taken from a MC simulation of the non-$Y(2175)$ process.

Figure 3 shows the projections of the simultaneous fit and their sum. The mass and width of the $Y(2175)$ are determined to be (2135 ± 8) MeV/c^2 and (104 ± 24) MeV, respectively, where the uncertainties are statistical only. The joint statistical significance of the $Y(2175)$ signal is estimated to be larger than 10σ by comparing the log-likelihood values with and without the $Y(2175)$ signal included in the fit and

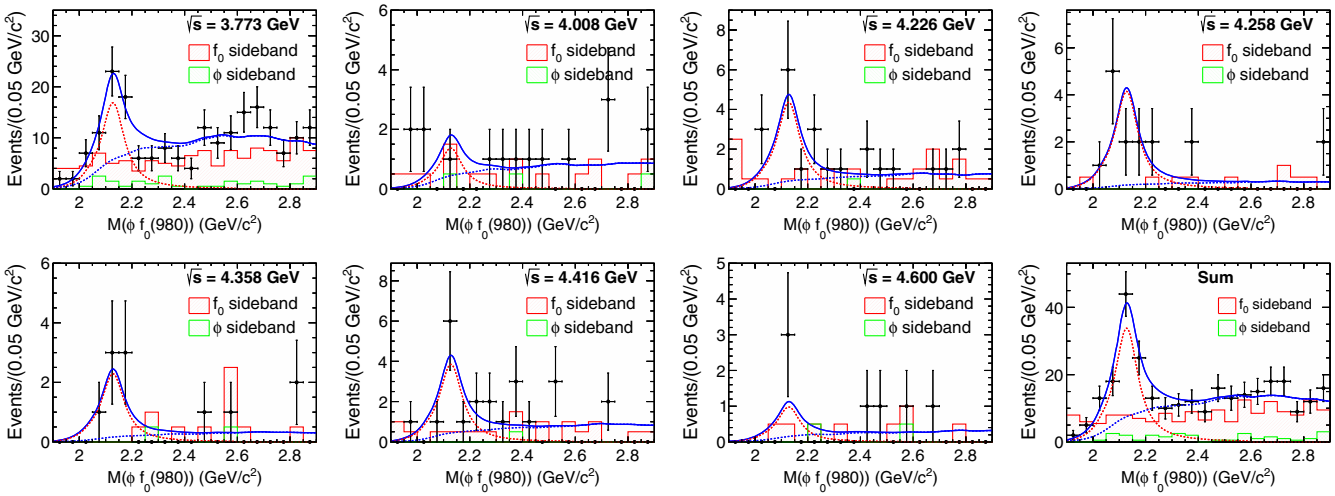

FIG. 3. Invariant mass distributions of $\phi f_0(980)$ and the projections of the simultaneous fit described in the text (solid curve) at the different c.m. energies, as well as the sum of them (bottom right, marked as "Sum"). The dots with error bars are data and the horizontal error bars indicate the bin width. The red dotted curves represent the Breit-Wigner functions for the signal and the blue dashed curves represent the background contributions, which are modeled by the MC distribution for the non-$Y(2175)$ background. The red and green histograms represent the normalized events from the $f_0(980)$ and ϕ mass sideband regions.

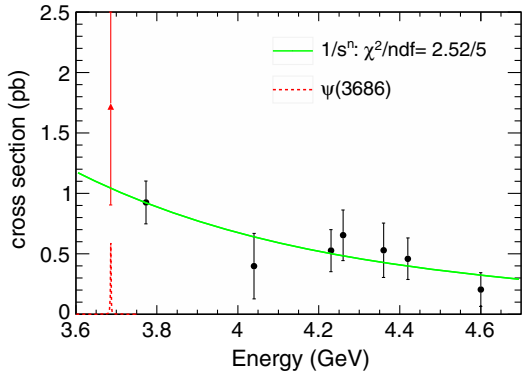

FIG. 4. Distribution of the Born cross sections for $e^+e^- \to \eta Y(2175)$. The red triangle represents the data at 3.686 GeV and black dots represent the other data samples. The solid green curve shows the fit result from data samples with $\sqrt{s} > 3.7$ GeV using the shape of Eq. (3) and the red dashed curve shows the contribution from $\psi(3686)$ as described in Sec. VI.

considering the change of the number of degrees of freedom. For each data sample, the statistical significance is estimated separately by fitting with and without the $Y(2175)$ signal included while the resonance parameters of the $Y(2175)$ are fixed to the values of the simultaneous fit. The numbers of signal events and the statistical significances are listed in Table I.

The Born cross section $\sigma^{\rm B}$ of $e^+e^- \to \eta Y(2175) \to \eta\phi f_0(980) \to \eta\phi\pi^+\pi^-$ is calculated using

$$\sigma^{\rm B} = \frac{\sigma^{\rm obs}}{(1+\delta)(1+\delta^{\rm vac})} = \frac{N^{\rm obs}}{\mathcal{L}_{\rm int}\mathcal{B}\epsilon(1+\delta)(1+\delta^{\rm vac})}, \quad (2)$$

where $\sigma^{\rm obs}$ is the observed cross section including the branching fraction $\mathcal{B}(Y(2175) \to \phi f_0(980) \to \phi\pi^+\pi^-)$; $N^{\rm obs}$ is the number of signal events; $\mathcal{L}_{\rm int}$ is the integrated luminosity; $\mathcal{B}$ is the product of branching fractions of $\eta \to \gamma\gamma$ and $\phi \to K^+K^-$; ϵ is the reconstruction efficiency; and $(1+\delta)$ is the ISR correction factor, including ISR, e^+e^- self-energy and initial vertex corrections. The vacuum polarization factor $(1+\delta^{\rm vac})$, including leptonic and hadronic contributions, is taken from Ref. [38].

The vector-pseudoscalar (VP) processes $e^+e^- \to VP$ are predicted to have Born cross sections that vary as $1/s^n$ [39] in the absence of contributions from charmonium(like) resonances. Here n is a parameter describing the energy-dependent form factor of $e^+e^- \to VP$. In calculating the ISR correction factors [40], the Born cross section of $e^+e^- \to \eta Y(2175)$ from threshold to the c.m. energy under study is needed as input. We assume that the $\eta Y(2175)$ comes from a QED process without the contribution from any charmonium(like) resonances, and the cross section is parametrized as

$$\sigma(s) \propto \frac{1}{s^n}. \quad (3)$$

Here n is obtained from a fit to the measured Born cross sections in this analysis. We use an iterative procedure to measure the Born cross sections and determine the ISR correction factors together with the efficiencies.

The resultant Born cross sections and all the numbers used in the calculation are listed in Table I and shown in Fig. 4. The fit to the final Born cross sections with Eq. (3) results in $n = 2.65 \pm 0.86$, as shown in Fig. 4, and the goodness of fit is $\chi^2/ndf = 2.52/5$.

V. SEARCH FOR Z_s STATES

Since we have observed a distinct $Y(2175)$ signal, possible charged Z_s states in the $\phi\pi^\pm$ invariant mass spectrum can be searched for in the $Y(2175)$ decays. In the cross section measurement, the candidate events are required to be within the $f_0(980)$ mass window to suppress the background. This requirement is released to include the non-$f_0(980)$ decay of $Y(2175)$ in the search for the Z_s states. The events in the $Y(2175)$ signal region, $[1.989, 2.272]$ GeV/c^2 in the $\phi\pi^+\pi^-$ invariant mass, are

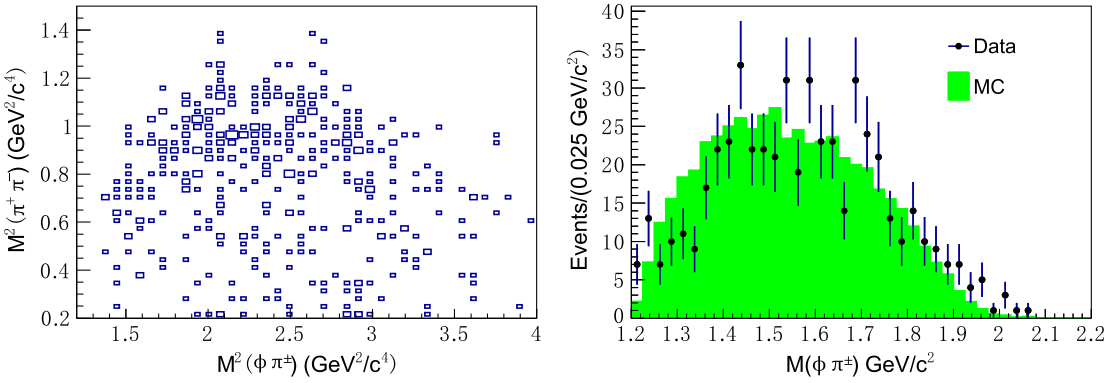

FIG. 5. Dalitz plot (left) and projection on $M(\phi\pi^\pm)$ (right) of $Y(2175) \to \phi\pi^+\pi^-$ events for the sum of all data samples at $\sqrt{s} > 3.7$ GeV (two entries per event). The green histogram in the right plot shows the same distribution for the normalized exclusive MC samples of the non-Z_s process.

selected and the Dalitz plot of $Y(2175) \to \phi\pi^+\pi^-$ events for the sum of data samples at $\sqrt{s} > 3.7$ GeV is shown in Fig. 5 (left). A clear $f_0(980)$ band in the horizontal direction is observed which dominates the $Y(2175) \to \phi\pi^+\pi^-$ decays. Figure 5 (right) shows the projection on the $\phi\pi^\pm$ invariant mass, $M(\phi\pi^\pm)$, for data and MC simulations of the non-Z_s process, which covers all the energy points and is normalized according to the luminosity and the fit result in Fig. 4; no obvious structure for data is observed.

From the theoretical calculation [20], which assumes that the Z_s states are $K\bar{K}^*$ and $K^*\bar{K}^*$ molecular states, the masses of Z_s states are expected at around 1.4 and 1.7 GeV/c^2, respectively. No significant vertical bands can be seen at the expected positions. We do not give quantitative results on the Z_s production due to the limited statistics and the poorly defined masses and widths of these states.

It is worth noting that the $Y(2175)$ signal produced in $e^+e^- \to \eta Y(2175)$ at $\sqrt{s} > 3.7$ GeV has a much lower background level compared with those in the other two known production processes, i.e., e^+e^- annihilation around the $Y(2175)$ peak [2,3,6] and $J/\psi \to \eta Y(2175)$ [4,5], though the signal yield is not comparable to the latter two processes at BESIII. With more data accumulated at $\sqrt{s} > 3.7$ GeV, the Z_s states could be searched for with high sensitivity via $e^+e^- \to \eta Y(2175)$.

VI. SEARCH FOR $\psi(3686) \to \eta Y(2175)$

With the same selections as those described in Sec. III, the $\phi f_0(980)$ invariant mass distribution at $\sqrt{s} = 3.686$ GeV is shown in Fig. 6. In contrast to the distributions at $\sqrt{s} > 3.7$ GeV, no significant $Y(2175)$ signal is observed. Given the difference in integrated luminosities,

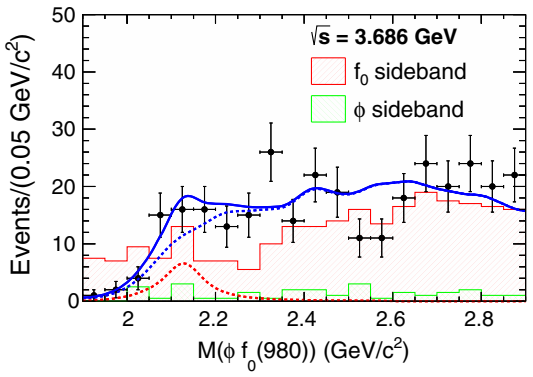

FIG. 6. Invariant mass distribution of $\phi f_0(980)$ at $\sqrt{s} = 3.686$ GeV and the fit result (solid curve). The dots with error bars are data and the horizontal error bars indicate the bin width. The red dashed curve represents the Breit-Wigner function for the signal and the blue dashed curve represents the background contribution, which is modeled by the MC simulation for the non-$Y(2175)$ background. The red and green histograms represent the events from the $f_0(980)$ and ϕ mass sideband regions.

the background level is much higher than that at other energies, indicating that $\psi(3686)$ decays are the main background.

The inclusive MC sample at $\sqrt{s} = 3.686$ GeV is used to check for possible backgrounds. No peaking background is found and the main background is the non-$Y(2175)$ process $\psi(3686) \to \eta K^+K^-\pi^+\pi^-$ (as well as a small fraction of $e^+e^- \to \eta K^+K^-\pi^+\pi^-$ through continuum production), including both the $\eta\phi\pi^+\pi^-$ and $\eta K^+K^- f_0(980)$ processes, and there are no other kinds of background around the $Y(2175)$ peak area. Exclusive MC samples of non-$Y(2175)$ processes from $\psi(3686)$ decays are generated with the same procedure described in Sec. III, and the shapes used to describe the background in the fit of the invariant mass distribution are as in the analysis of data samples at $\sqrt{s} > 3.7$ GeV.

The same fit functional forms for signal and background as in the fit to the data samples at $\sqrt{s} > 3.7$ GeV (Sec. IV) are used to determine the signal yield of $Y(2175)$. Since the signal yield of $Y(2175)$ is very small, we fix the mass and width of the $Y(2175)$ to the values obtained in the fit to the data samples at $\sqrt{s} > 3.7$ GeV. The fit returns 19.0 ± 9.0 events of $Y(2175)$ signal with a statistical significance of 1.5σ, and the fit curve is shown in Fig. 6. The Born cross section and the numbers used to calculate it are listed in Table I. The obtained Born cross section is consistent with the extrapolation of the cross section variation fitted to those at $\sqrt{s} > 3.7$ GeV, which is the green curve in Fig. 4, within the large uncertainty. This consistency indicates that the $Y(2175)$ production at $\sqrt{s} = 3.686$ GeV is dominated by the QED continuum process since it is the only process considered in the cross section variation [Eq. (3)].

As the process $J/\psi \to \eta Y(2175)$ has been observed [4,5], we expect the production of $\psi(3686) \to \eta Y(2175)$ to occur as well, although there is no guideline for a prediction of the decay branching fraction. As described in Sec. IV, the obtained Born cross sections for the data samples at $\sqrt{s} > 3.7$ GeV are fitted based on an assumption that no charmonium(like) resonances above the open-charm threshold contribute to this decay. Hence the extrapolation from the fit result, which is shown as the green curve in Fig. 4, is used to estimate the contribution from the QED continuum process at $\sqrt{s} = 3.686$ GeV. After subtracting the contribution from the QED process (assuming there is no interference between the resonance and QED processes [41]), we obtain the product $\sigma(e^+e^- \to \psi(3686)) \cdot \mathcal{B}(\psi(3686) \to \eta Y(2175) \to \eta\phi f_0(980) \to \eta\phi\pi^+\pi^-)$ to be (0.68 ± 0.82) pb with the number of signal events estimated to be 7.5 ± 9.0, where the errors are statistical only. The corresponding contribution of $\psi(3686)$ in the cross section is parametrized as a Breit-Wigner function convolved with a Gaussian function which represents the beam energy spread, and it is shown as the red dashed curve in Fig. 4. The efficiency, 10.7%, is obtained from an exclusive MC simulation of $\psi(3686) \to \eta Y(2175) \to \gamma\gamma\pi^+\pi^- K^+K^-$.

Using the total number of produced $\psi(3686)$ events ($(448.1 \pm 2.9) \times 10^6$) [24], we obtain $\mathcal{B}(\psi(3686) \to \eta Y(2175)) \cdot \mathcal{B}(Y(2175) \to \phi f_0(980) \to \phi\pi^+\pi^-)$ to be $(0.81 \pm 0.97) \times 10^{-6}$, or less than 2.2×10^{-6} at the 90% confidence level (C.L.), where the systematic uncertainty, which will be detailed later, has been included. The Bayesian method, as described in Ref. [42], is used to estimate the upper limit.

Using $\mathcal{B}(J/\psi \to \eta Y(2175)) \cdot \mathcal{B}(Y(2175) \to \phi f_0(980) \to \phi\pi^+\pi^-) = (1.20 \pm 0.14(\text{stat}) \pm 0.37(\text{syst})) \times 10^{-4}$ from the previous BESIII's measurement [5], the ratio of the reduced branching fractions $\mathcal{B}^*(\psi(3686) \to \eta Y(2175))/\mathcal{B}^*(J/\psi \to \eta Y(2175))$ is found to be $(0.23 \pm 0.29)\%$ after considering the two-body P-wave phase space difference between $\psi(3686)$ and J/ψ decays, or less than 0.65% at the 90% C.L. after considering the uncertainty of $\mathcal{B}(J/\psi \to \eta Y(2175))$. Here the uncertainty is statistical only.

VII. SEARCH FOR $e^+e^- \to \eta' Y(2175)$

In the search for $e^+e^- \to \eta' Y(2175)$, we use the same final state to reconstruct the $Y(2175)$ as in the $e^+e^- \to \eta Y(2175)$ case, and we use the decay mode $\gamma\pi^+\pi^-$ to reconstruct the η'. The event selection therefore requires four charged pions and two charged kaons and at least one photon. To classify these particles, we first use PID to separate kaons from pions, and utilize the kinematic fit to the final state particles to identify the $\pi^+\pi^-$ combination from the η' decays, constraining the $\gamma\pi^+\pi^-$ invariant mass to be the nominal η' mass [1]. We loop over all the $\pi^+\pi^-$ combinations, and the one with the smallest χ^2 is retained. In order to use the information of the η' sideband for further study, the η' mass constraint is released after the $\pi^+\pi^-$ from η' decays is identified and the χ^2 of the kinematic fit is required to be less than 60. The mass window of η' ($[0.943, 0.971]$ GeV/c^2 in the $\gamma\pi^+\pi^-$ invariant mass) as well as those of $f_0(980)$ and ϕ, defined in Sec. III, are used to select the signal events.

After all the above event selections are applied, the distribution of the $\phi f_0(980)$ invariant mass, $M(\phi f_0(980))$, for the sum of data samples at $\sqrt{s} > 3.7$ GeV is shown in Fig. 7. The data sample at $\sqrt{s} = 3.686$ GeV is not used due to the low integrated luminosity and the relatively high background level. Also shown in Fig. 7 are the distributions of the events in the η', $f_0(980)$ and ϕ sideband regions as defined in Sec. III. There are only a few events at $M(\phi f_0(980))$ around 2.1 GeV/c^2 and no significant $Y(2175)$ or any other structure is observed. Events from the sidebands can describe the events in the signal region reasonably well. The inclusive MC sample at $\sqrt{s} = 3.773$ GeV is used to check the background and no peaking background is found.

The Bayesian method described in Ref. [42] is used to set an upper limit. We use the $e^+e^- \to \eta' Y(2175)$ signal MC simulation described in Sec. II for the signal shape and a second-order polynomial function for the background shape. An upper limit of 27.6 events is obtained at the 90% C.L. after considering the systematic uncertainties.

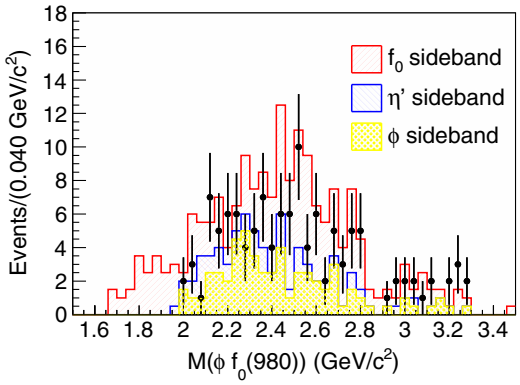

FIG. 7. Distribution of $\phi f_0(980)$ invariant mass, $M(\phi f_0(980))$, for the sum of data samples at $\sqrt{s} > 3.7$ GeV. The red, blue and yellow histograms are the events in the sideband regions of $f_0(980)$, η' and ϕ, respectively.

The upper limit on the ratio $R = \sigma_{\eta' Y(2175)}/\sigma_{\eta Y(2175)}$, where $\sigma_{\eta' Y(2175)}$ and $\sigma_{\eta Y(2175)}$ are the cross sections of $e^+e^- \to \eta' Y(2175)$ and $\eta Y(2175)$ processes, respectively, is determined by assuming this ratio is the same at different c.m. energy points, that is,

$$R = \frac{N^{\text{obs}}_{\eta' Y(2175)}}{N^{\text{obs}}_{\eta Y(2175)}} \cdot \frac{\mathcal{B}_\eta}{\mathcal{B}_{\eta'}} \cdot \frac{\sum_i \sigma^i_{\eta Y(2175)} \cdot \mathcal{L}^i_{\text{int}} \cdot \epsilon^i_{\eta Y(2175)} \cdot (1+\delta)^i \cdot (1+\delta^{\text{vac}})^i}{\sum_j \sigma^j_{\eta Y(2175)} \cdot \mathcal{L}^j_{\text{int}} \cdot \epsilon^j_{\eta' Y(2175)} \cdot (1+\delta)^j \cdot (1+\delta^{\text{vac}})^j}. \quad (4)$$

Here N^{obs} is the number of observed $\eta Y(2175)$ (95.0 ± 12.1) or $\eta' Y(2175)$ events from the sum of the seven data samples at $\sqrt{s} > 3.7$ GeV; $\sigma^{i(j)}_{\eta Y(2175)}$ and $\mathcal{L}^{i(j)}_{\text{int}}$ are the Born cross section for $e^+e^- \to \eta Y(2175)$ as shown in Eq. (2) and the integrated luminosity for the $i(j)$th data sample; and $\epsilon_{\eta Y(2175)}$ and $\epsilon_{\eta' Y(2175)}$ are the signal reconstruction efficiencies for the $e^+e^- \to \eta Y(2175)$ and $\eta' Y(2175)$ processes, respectively, obtained from the signal MC simulation samples. These numbers are listed in Table I. Also, $\mathcal{B}_\eta$ and $\mathcal{B}_{\eta'}$ are the branching fractions of $\eta \to \gamma\gamma$ and $\eta' \to \gamma\pi^+\pi^-$ [1], respectively. With the numbers obtained above, the upper limit on the ratio R is estimated to be 0.43 at the 90% C.L., where the systematic uncertainties, which will be detailed later, are included.

VIII. SYSTEMATIC UNCERTAINTIES

A. Cross section measurement of $e^+e^- \to \eta Y(2175)$

Systematic uncertainties for the cross section measurement of $e^+e^- \to \eta Y(2175)$ are summarized in Table II and are discussed below.

TABLE II. Summary of systematic uncertainties (%) in $e^+e^- \to \eta Y(2175)$ cross section measurements for data samples at 8 different c.m. energies.

Source/$\sqrt{s}$ (GeV)	3.686	3.773	4.008	4.226	4.258	4.358	4.416	4.600
Luminosity	1.0	1.0	1.0	1.0	1.0	1.0	1.0	1.0
Tracking efficiency	4.0	4.0	4.0	4.0	4.0	4.0	4.0	4.0
Photon reconstruction efficiency	2.0	2.0	2.0	2.0	2.0	2.0	2.0	2.0
PID efficiency	2.0	2.0	2.0	2.0	2.0	2.0	2.0	2.0
Branching fraction	1.2	1.2	1.2	1.2	1.2	1.2	1.2	1.2
Radiative correction	2.6	4.2	2.4	6.5	5.1	2.7	2.6	3.7
Kinematic fit	0.4	0.3	0.4	0.4	0.4	0.4	0.4	0.6
Background shape	57.6	14.7	84.3	4.8	9.2	11.4	45.9	5.5
Parametrization of $f_0(980)$	1.1	1.1	1.1	1.1	1.1	1.1	1.1	1.1
Total	58.0	16.2	84.5	9.9	12.1	13.2	46.4	8.7

The luminosity is measured using large-angle Bhabha scattering with an uncertainty less than 1.0% [22]. The difference between data and MC simulation in the tracking efficiency is evaluated to be 1.0% per track, and that in the PID efficiency is 1.0% per track [42]. The uncertainty in the reconstruction efficiency for a photon is determined to be less than 1.0% by studying a sample of $J/\psi \to \rho\pi \to \pi^+\pi^-\pi^0$ events, and the energy and polar angle of the photon from η or η' in this analysis can be well covered by that of the photon from the π^0.

The branching fractions of the η and ϕ decays are taken from the world average values [1], and the corresponding uncertainties are taken as a systematic uncertainty. For the η and ϕ mass windows, the mass regions are taken to be $\pm 1.5 \cdot \mathrm{FWHM}$ from the nominal masses [1]; the efficiency difference due to any mass resolution difference between data and MC simulation is very small and can be neglected compared to other sources of uncertainties.

Since statistics are limited, the line shape of $e^+e^- \to \eta Y(2175)$ cannot be measured precisely. We assume there is no contribution from charmonium(like) states at $\sqrt{s} > 3.7$ GeV and parametrize the line shape to be proportional to $1/s^n$. While we take the mean value of n from a fit to the data with an iterative process, we vary n by one standard deviation and regenerate MC samples. The difference in $(1+\delta)\cdot\epsilon$ is taken as a systematic uncertainty.

We use the method described in Refs. [43,44] to estimate the uncertainties introduced by the kinematic fit. The helix parameters of the tracks in the MC sample have been corrected empirically to best match the data. The corrected MC sample is used for the nominal results, and many other analyses have shown that there is good agreement between data and the corrected samples. We assign half the difference between the results obtained with and without these corrections as the systematic uncertainty on the cross sections. This uncertainty is around 0.4% for all the data samples.

In the nominal fit, the shape from simulation of the non-$Y(2175)$ process $e^+e^- \to \eta K^+K^-\pi^+\pi^-$ is taken to describe the background. We change the shape of the background to be a second order polynomial function for data with $\sqrt{s} > 3.7$ GeV and to a shape from the inclusive MC sample for the data at $\sqrt{s} = 3.686$ GeV, and we take the difference in signal yields as the systematic uncertainties due to background shape. The uncertainty due to signal parametrization is obtained by altering the signal shape into an S-wave Breit-Wigner function with a mass-dependent width since $Y(2175)$ has $J^{PC} = 1^{--}$ and it is expected to decay to $\phi f_0(980)$ in a relative S-wave. It is found to be negligible compared with that from the background shape. The systematic uncertainty associated with the fit range is studied by changing the fit range by 100 MeV/c^2. The resultant value is 0.5% only and is neglected.

The Flatté formula [29] is used to model the $f_0(980)$ line shape in MC generation, where the parameters of $f_0(980)$ are taken from the BESII measurement [30]. To estimate the corresponding systematic uncertainty, we vary the parameters by one standard deviation from the central values and the resultant difference in efficiency is taken as the systematic uncertainty.

Assuming all the sources of uncertainty are independent, the total uncertainty is obtained by summing all the individual uncertainties in quadrature, and it is summarized in Table II.

B. Mass and width of the $Y(2175)$

The systematic uncertainties for the mass and width of the $Y(2175)$ include those from the mass calibration, signal shape of the $Y(2175)$, background shape and c.m. energy.

A kinematic fit is performed with energy-momentum conservation, so we can use the mass of η to calibrate the mass of the $Y(2175)$. A simultaneous fit is performed on $\gamma\gamma$ invariant mass distributions for all the data samples. The difference between the fitted mass and the nominal mass [1], 2.1 MeV/c^2, is taken as the systematic uncertainty.

An S-wave Breit-Winger function with mass-dependent width, the same as the function described in Sec. VIII A, is used to parametrize the $Y(2175)$ shape in the fit, yielding a

mass difference of 2.5 MeV/c^2 and a width difference of 1.5 MeV. The mass resolution is about 4.5 MeV/c^2, which is much smaller than the width of $Y(2175)$, and the corresponding effect on width measurement is found to be negligible.

In the nominal fit, we use the shape from the simulated non-$Y(2175)$ MC events to describe the background. To study the corresponding systematic uncertainty, as described in Sec. VIII A, we change the background shape to a second-order polynomial function and the resultant differences in the fitted mass and width, 8.2 MeV/c^2 and 12.1 MeV, respectively, are taken as systematic uncertainties.

The c.m. energy of the e^+e^- system also affects the determination of the mass and width of the $Y(2175)$ due to the kinematic constraint between initial and final states. An analysis [21] reveals that the uncertainty on the c.m. energy of e^+e^- is less than 0.8 MeV. We change the c.m. energy by ± 0.8 MeV in the kinematic fit and study the changes of mass and width, which are 0.2 MeV/c^2 and 0.4 MeV, respectively.

The quadratic sum of all the above uncertainties, 8.8 MeV/c^2 and 12.2 MeV for the mass and width, respectively, is taken as the total uncertainties.

C. Branching fraction $\mathcal{B}(\psi(3686) \to \eta Y(2175)) \cdot \mathcal{B}(Y(2175) \to \phi f_0(980) \to \phi\pi^+\pi^-)$

The sources of systematic uncertainties on the product of branching fractions $\mathcal{B}(\psi(3686) \to \eta Y(2175)) \cdot \mathcal{B}(Y(2175) \to \phi f_0(980) \to \phi\pi^+\pi^-)$ are the same as those in the cross section measurement. An additional uncertainty associated with the total number of $\psi(3686)$ events [24], 0.65%, is also taken into account. The systematic uncertainty due to QED continuum background estimation is obtained by altering one standard deviation for the parameter n of the line shape parametrization function $1/s^n$, and it is found to be negligible. The resultant systematic uncertainty for the branching fraction product $\mathcal{B}(\psi(3686) \to \eta Y(2175)) \cdot \mathcal{B}(Y(2175) \to \phi f_0(980) \to \phi\pi^+\pi^-)$ is 58.0%.

The systematic uncertainty on the ratio of branching fraction $\mathcal{B}(\psi(3686) \to \eta Y(2175))/\mathcal{B}(J/\psi \to \eta Y(2175))$ is assigned from the quadratic sum of the relative systematic uncertainties of $\mathcal{B}(\psi(3686) \to \eta Y(2175))$ and $\mathcal{B}(J/\psi \to \eta Y(2175))$, since they are measured with different data samples and different fit methods.

D. Ratio $R = \sigma(e^+e^- \to \eta' Y(2175))/\sigma(e^+e^- \to \eta Y(2175))$

For the ratio R, the systematic uncertainties related to the signal shape, radiative correction, luminosity and some selections in the $Y(2175)$ reconstruction are common for $e^+e^- \to \eta Y(2175)$ and $\eta' Y(2175)$ and can be canceled. The remaining uncertainties arise from the differences between η and η', i.e., decay branching fractions and reconstruction efficiencies, where η is reconstructed from two photons and η' from one photon and two charged pions. The fraction of common systematic uncertainty introduced by the kinematic fit is hard to estimate. We assume they are independent and add them in quadrature. The systematic uncertainty due to the background shape, 48.7%, is obtained by varying the shape to that determined by the events in the sideband regions of η' and ϕ. We assume that all the sources of systematic uncertainty are independent and obtain the total uncertainty on R to be 50.6% by adding the statistical and systematic uncertainties in quadrature. The total uncertainty is used in calculating the upper limit of R.

IX. SUMMARY

We observe clear $Y(2175)$ signals in the process $e^+e^- \to \eta Y(2175)$ using data samples at $\sqrt{s} = 3.773$, 4.008, 4.226, 4.258, 4.358, 4.416, and 4.600 GeV. In the measured c.m.-energy-dependent Born cross sections, no obvious peaks corresponding to decays of charmonium(like) states to the final state $\eta Y(2175)$ are seen. The mass and width of the $Y(2175)$ are measured to be $(2135 \pm 8 \pm 9)$ MeV/c^2 and $(104 \pm 24 \pm 12)$ MeV, respectively, where the first uncertainties are statistical and the second systematic. Comparing to the world average values [1], the obtained parameters of the $Y(2175)$ have similar precision and are consistent considering the large uncertainties. An examination of the Dalitz plot of the $Y(2175) \to \phi\pi^+\pi^-$ indicates that $\phi f_0(980)$ is a dominant component, and no obvious signal of a potential charged strangeoniumlike state $Z_s^\pm \to \phi\pi^\pm$ is observed.

The cross section of $e^+e^- \to \eta Y(2175)$ varies with the c.m. energy as $1/s^n$ with $n = 2.65 \pm 0.86$, which can be compared with measurements of other vector-pseudoscalar final states and theoretical calculations [39,45]. The deviation from the behavior of final states with ordinary vector quarkonium states may reveal the nature of the $Y(2175)$, where theoretical calculations are expected for different assumptions of the parton configuration of the $Y(2175)$.

No significant $\psi(3686) \to \eta Y(2175)$ signal is observed, and the branching fraction product $\mathcal{B}(\psi(3686) \to \eta Y(2175)) \cdot \mathcal{B}(Y(2175) \to \phi f_0(980) \to \phi\pi^+\pi^-)$ is obtained to be $(0.81 \pm 0.97 \pm 0.47) \times 10^{-6}$, or less than 2.2×10^{-6} at the 90% C.L. The ratio of the branching fractions $\mathcal{B}^*(\psi(3686) \to \eta Y(2175))/\mathcal{B}^*(J/\psi \to \eta Y(2175))$ is $(0.23 \pm 0.29 \pm 0.13)$%, or less than 0.65% at the 90% C.L., after considering the phase space difference between $\psi(3686)$ and J/ψ decays to the $\eta Y(2175)$ final state. A large suppression of $\psi(3686) \to \eta Y(2175)$ with respect to the "12% rule" [41] is observed. This is therefore another vector-pseudoscalar channel failing the 12% rule.

With the same data samples, the process $e^+e^- \to \eta' Y(2175)$ is searched for. No significant signal is observed. We set the upper limit on the ratio of the cross

sections $\sigma(e^+e^- \to \eta' Y(2175))/\sigma(e^+e^- \to \eta Y(2175))$ to be 0.43 at the 90% C.L.

ACKNOWLEDGMENTS

The BESIII Collaboration thanks the staff of BEPCII and the IHEP computing center for their strong support. This work is supported in part by the National Key Basic Research Program of China under Contract No. 2015CB856700; National Natural Science Foundation of China (NSFC) under Contracts No. 10979033, No. 11235011, No. 11335008, No. 11425524, No. 11625523, and No. 11635010; the Chinese Academy of Sciences (CAS) Large-Scale Scientific Facility Program; the CAS Center for Excellence in Particle Physics (CCEPP); Joint Large-Scale Scientific Facility Funds of the NSFC and CAS under Contracts No. U1332201, No. U1532257, and No. U1532258; CAS under Contracts No. KJCX2-YW-N29, No. KJCX2-YW-N45, and No. QYZDJ-SSW-SLH003; 100 Talents Program of CAS; New Century Excellent Talents in University (NCET) under Contract No. NCET-13-0342; Shandong Natural Science Funds for Distinguished Young Scholar under Contact No. JQ201402; National 1000 Talents Program of China; INPAC and Shanghai Key Laboratory for Particle Physics and Cosmology; German Research Foundation DFG under Contracts No. Collaborative Research Center CRC 1044 and No. FOR 2359; Istituto Nazionale di Fisica Nucleare, Italy; Koninklijke Nederlandse Akademie van Wetenschappen (KNAW) under Contract No. 530-4CDP03; Ministry of Development of Turkey under Contract No. DPT2006K-120470; National Science and Technology fund; the Swedish Research Council; U.S. Department of Energy under Contracts No. DE-FG02-05ER41374, No. DE-SC-0010118, No. DE-SC-0010504, and No. DE-SC-0012069; University of Groningen (RuG) and the Helmholtzzentrum fuer Schwerionenforschung GmbH (GSI), Darmstadt; and the WCU Program of the National Research Foundation of Korea under Contract No. R32-2008-000-10155-0.

[1] C. Patrignani *et al.* (Particle Data Group), Chin. Phys. C **40**, 100001 (2016).
[2] B. Aubert *et al.* (*BABAR* Collaboration), Phys. Rev. D **74**, 091103(R) (2006).
[3] C. P. Shen *et al.* (Belle Collaboration), Phys. Rev. D **80**, 031101(R) (2009).
[4] M. Ablikim *et al.* (BES Collaboration), Phys. Rev. Lett. **100**, 102003 (2008).
[5] M. Ablikim *et al.* (BESIII Collaboration), Phys. Rev. D **91**, 052017 (2015).
[6] J. P. Lees *et al.* (*BABAR* Collaboration), Phys. Rev. D **86**, 012008 (2012).
[7] Z. G. Wang, Nucl. Phys. **A791**, 106 (2007).
[8] H. X. Chen, X. Liu, A. Hosaka, and S.-L. Zhu, Phys. Rev. D **78**, 034012 (2008).
[9] G. J. Ding and M. L. Yan, Phys. Lett. B **650**, 390 (2007).
[10] G. J. Ding and M. L. Yan, Phys. Lett. B **657**, 49 (2007).
[11] X. Wang, Z.-F. Sun, D.-Y. Chen, X. Liu, and T. Matsuki, Phys. Rev. D **85**, 074024 (2012).
[12] S. Godfrey and N. Isgur, Phys. Rev. D **32**, 189 (1985).
[13] T. Barnes, F. E. Close, P. R. Page, and E. S. Swanson, Phys. Rev. D **55**, 4157 (1997).
[14] T. Barnes, N. Black, and P. R. Page, Phys. Rev. D **68**, 054014 (2003).
[15] M. Ablikim *et al.* (BESIII Collaboration), Phys. Rev. Lett. **110**, 252001 (2013).
[16] M. Ablikim *et al.* (BESIII Collaboration), Phys. Rev. Lett. **111**, 242001 (2013).
[17] M. Ablikim *et al.* (BESIII Collaboration), Phys. Rev. Lett. **112**, 022001 (2014).
[18] M. Ablikim *et al.* (BESIII Collaboration), Phys. Rev. Lett. **112**, 132001 (2014).
[19] A. Bondar *et al.* (Belle Collaboration), Phys. Rev. Lett. **108**, 122001 (2012).
[20] D. Y. Chen, X. Liu, and T. Matsuki, Eur. Phys. J. C **72**, 2008 (2012).
[21] M. Ablikim *et al.* (BESIII Collaboration), Chin. Phys. C **40**, 063001 (2016).
[22] M. Ablikim *et al.* (BESIII Collaboration), Chin. Phys. C **39**, 093001 (2015).
[23] M. Ablikim *et al.* (BESIII Collaboration), Nucl. Instrum. Methods Phys. Res., Sect. A **614**, 345 (2010).
[24] M. Ablikim *et al.* (BESIII Collaboration), Chin. Phys. C **42**, 023001 (2018).
[25] S. Agostinelli *et al.* (GEANT4 Collaboration), Nucl. Instrum. Methods Phys. Res., Sect. A **506**, 250 (2003).
[26] Z. Y. Deng *et al.*, High Energy Phys. Nucl. Phys. **30**, 371 (2006).
[27] D. J. Lange, Nucl. Instrum. Methods Phys. Res., Sect. A **462**, 152 (2001).
[28] R. G. Ping, Chin. Phys. C **32**, 599 (2008).
[29] S. M. Flatté, Phys. Lett. **63B**, 224 (1976).
[30] M. Ablikim *et al.* (BES Collaboration), Phys. Lett. B **607**, 243 (2005).
[31] S. Jadach, B. F. L. Ward, and Z. Was, Comput. Phys. Commun. **130**, 260 (2000); Phys. Rev. D **63**, 113009 (2001).
[32] E. Barberio and Z. Was, Comput. Phys. Commun. **79**, 291 (1994).
[33] J. Libby *et al.* (CLEO Collaboration), Phys. Rev. Lett. **101**, 182002 (2008).

[34] J. C. Chen, G. S. Huang, X. R. Qi, D. H. Zhang, and Y. S. Zhu, Phys. Rev. D **62**, 034003 (2000).
[35] T. Sjöstrand *et al.*, arXiv:hep-ph/0108264.
[36] S. Nova, A. Olshevski, and T. Todorov, CERN, Report No. DELPHI 90-35, 1990.
[37] G. Balossini, C. M. Carioni Calame, G. Montagna, O. Nicrosini, and F. Piccinini, Nucl. Phys. **B758**, 227 (2006).
[38] S. Actis *et al.* Eur. Phys. J. C **66**, 585 (2010).
[39] C. D. Lu, W. Wang, and Y. M. Wang, Phys. Rev. D **75**, 094020 (2007).
[40] E. A. Kuraev and V. S. Fadin, Yad. Fiz. **41**, 733 (1985).
[41] X. H. Mo, C. Z. Yuan, and P. Wang, High Energy Phys. Nucl. Phys. **31**, 686 (2007).
[42] M. Ablikim *et al.* (BESIII Collaboration), Phys. Rev. D **91**, 032002 (2015).
[43] M. Ablikim *et al.* (BESIII Collaboration), Phys. Rev. D **91**, 112005 (2015).
[44] M. Ablikim *et al.* (BESIII Collaboration), Phys. Rev. D **87**, 012002 (2013).
[45] C. P. Shen *et al.* (Belle Collaboration), Phys. Rev. D **88**, 052019 (2013).